CrystEngComm

PAPER

View Article Online
View Journal | View Issue

Cite this: *CrystEngComm*, 2023, **25**, 3718

Numerical analysis of the dislocation density in n-type 4H-SiC

Sheng'ou Lu, [ac] Hongyu Chen,[a] Wei Hang,[a] Rong Wang, [bc] Julong Yuan,*[a] Xiaodong Pi, *[bc] Deren Yang [bc] and Xuefeng Han*[bc]

Received 9th March 2023,
Accepted 22nd May 2023

DOI: 10.1039/d3ce00219e

rsc.li/crystengcomm

A 4H-SiC single crystal is a substrate material for high-frequency and high-voltage power devices. Dislocation density is a fundamental criterion for evaluating the quality of 4H-SiC single crystals. 4H-SiC single crystals grown by the physical vapor transport (PVT) method generally have high dislocation density. To investigate the effect of nitrogen doping on dislocation proliferation in SiC crystals, the thermal field of the ingot during PVT growth was calculated by COMSOL Multiphysics, and thermal stress was calculated by thermal elastic theory. Finally, the dislocation density of the crystal was calculated based on the Alexander–Haasen model for inhomogeneous nitrogen doping. By comparing the calculation and experimental results, we proposed a possible value of the effective stress to evaluate the effect of a nitrogen dopant on dislocation density, which helps calculate the dislocation density in the n-type SiC.

1. Introduction

Silicon carbide (SiC) is one of the wide-bandgap semiconductors which has received much attention due to its excellent properties, such as a high breakdown field strength, high thermal conductivity, and high carrier saturation mobility.[1–3] There are more than 200 different polytypes of SiC crystals, of which 4H-SiC has received considerable attention due to its excellent electrical properties.[4] The effective n-type doping of 4H-SiC can be readily carried out by doping nitrogen (N) because the ionization energy of N is relatively tiny (~0.06 eV).[3] The first technological milestone was the introduction of the SiC Schottky diode by Infineon in 2001, followed by rapid market growth leading to the development of a family of diodes with voltage ratings ranging from 600 V to 3 kV.[1] Then, the release of CREE's first SiC MOSFET in 2011 definitively accelerated the adoption of SiC devices in numerous applications, such as electric vehicles, photovoltaics, and high-speed rail transportation. Physical vapor transport (PVT) is the current mainstream method for growing single SiC crystals. However, there are still many dislocations in the crystal prepared by this method, which will seriously affect the yield of the devices. Therefore, the dislocation density is one of the most important criteria for assessing the quality of the crystal.

To better understand the dislocation behavior in the n-type SiC, researchers employed the Alexander–Haasen[5,6] (AH) model to accurately calculate time-dependent plastic deformations of III–V compound[7] semiconductor materials over a wide range of stresses and temperatures. B. Gao *et al.*[8] have demonstrated through simulations and experiments that the AH model also applies to the plastic deformation of IV–IV compound semiconductor materials such as SiC. Some studies use the AH model to calculate the dislocation density in the SiC without impurities.[8–12] However, there is no reflection on calculating the dislocation density in n-type 4H-SiC.

In this work, we apply the AH model to calculate the dislocation density of n-type 4H-SiC by considering the pinning effect of nitrogen impurities on the dislocation. The experiment of intended nitrogen doping is used to validate our calculation. By comparing the calculation and experimental results, we propose an effective stress suitable for calculating the dislocation density at a certain doping concentration. This method provides a basis for predicting the dislocation density of n-type SiC.

2. Modeling and experimental

2.1 Geometric model

Fig. 1a is a 2D axis-symmetric global model for the PVT growth of a SiC single crystal with a crystal diameter of 100 mm. Crystal growth was conducted in an induction-heating furnace. Induction heating coils with a frequency of 10 kHz

[a] *Ultra-precision Machining Research Center, Zhejiang University of Technology, Hangzhou 310023, China. E-mail: jlyuan@zjut.edu.cn*
[b] *State Key Laboratory of Silicon Materials & School of Materials Science and Engineering, Zhejiang University, Hangzhou 311200, China. E-mail: xdpi@zju.edu.cn, xuefenghan@zju.edu.cn*
[c] *Institute of Advanced Semiconductors & Zhejiang Provincial Key Laboratory of Power Semiconductor Materials and Devices, Hangzhou Global Scientific and Technological Innovation Center, Zhejiang University, Hangzhou, Zhejiang 310027, China*

Published on 23 May 2023. Downloaded by Xiamen University on 4/11/2024 1:34:50 PM.

This journal is © The Royal Society of Chemistry 2023

Published on 23 May 2023. Downloaded by Xiamen University on 4/11/2024 1:34:50 PM.

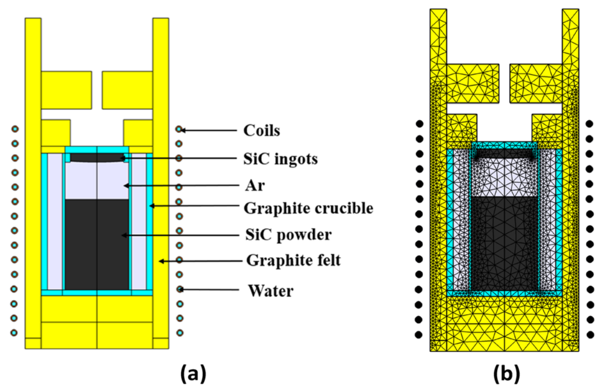

Fig. 1 The crystal growth system in finite element calculations: (a) global model for PVT growth of the 4H-SiC single crystal. (b) The meshing of the calculation model.

were used to heat the SiC powder, and cooling water pipes with a temperature of 300 K were inside the induction heating coils. The furnace was filled with argon gas at a fixed pressure of 1000 Pa. The graphite crucible is wrapped in graphite felts, which are excellent insulation materials. Fig. 1b shows the meshing of the finite element computational model using the built-in physical field control mesh in the program. A free triangular mesh is used to mesh the solution domain.

We first calculate the thermal field of crystal growth, then calculate the stress distribution in SiC ingots based on thermoelastic theory and finally calculate the dislocation density in the crystal based on the Alexander–Haasen model. Fig. 2 shows the sequence of the calculation procedure. In the following subsections, the principles for modeling the thermal, stress, and dislocation fields, as well as the corresponding governing equations and boundary conditions, are presented in turn.

2.2 Heat transfer

It is essential first to examine the strength of various parameters in a SiC growth system. The physical meaning of the Grashof number is the ratio of the buoyant force to the viscous force, which is expressed as follows:

$$G_r = \frac{g\alpha_v \Delta T L^3}{\nu^2} \tag{1}$$

where g is the gravitational acceleration; α_v is the isobaric expansion coefficient of an ideal gas; ΔT is the temperature difference; L is the characteristic length representing the inner diameter of the crucible; ν is kinematic viscosity.

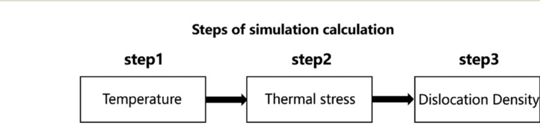

Fig. 2 Operation flow chart of the simulation calculation.

The Grashof number is estimated to be between 3 and 24 for a crucible with an inner diameter of 50–100 mm (for the growth of 25–75 mm diameter crystals, current industry standard). The heat transfer by buoyancy flow in the present industrial growth system can be considered negligible.[13]

Global heat transfer processes include thermal conduction, convection, and radiation. Thermal conduction generally occurs in solids and gases, thermal convection manifests as the heat exchange of fluids due to natural or forced convection, and thermal radiation includes surface-to-surface and surface-to-environment radiation. The following equation describes the physical phenomenon of heat transfer:

$$\nabla \cdot q = Q \tag{2}$$

$$q = -k\nabla T \tag{3}$$

where T is temperature; q is local heat flux; k is thermal conductivity; Q is volumetric heat source.

Most experiments and simulations[13,14] have demonstrated that the contribution of thermal convection to the heat transfer in the PVT method can be neglected, so this model does not consider the effect of fluid flow on heat transfer.

The heat flux for the boundary conditions is calculated as follows:

$$q_w = \lambda \frac{T_w - T_c}{dx} \tag{4}$$

where λ is the thermal conductivity of the wall; T_w is the wall temperature, and T_c is growth chamber temperature.

The radiative heat flux at the wall is calculated under the heat transfer wall boundary condition as follows:

$$q_w = \varepsilon\sigma(T_{amb}^{\ 4} - T_w^{\ 4}) \tag{5}$$

where σ is the Stefan–Boltzmann constant; T_{amb} is the ambient temperature; T_w is the wall temperature and ε is the wall emissivity.

The values in the above formula can be found in Table 1.[15]

2.3 Thermal stress

The governing equations for calculating thermal stresses include mechanical equilibrium equations, strain compatibility equations, geometric equations, and the constitutive relation. Continuous temperature variations within a solid generally generate thermal stresses. According to the linear thermal stress theory, the components of the strain tensor are a linear function of the stress tensor, and the temperature variation generates the components of the strain tensor.

Hooke's law and stress–strain relations for elastic and thermal strains are given by:

$$\sigma_{ij} = C_{ijkl}(\varepsilon_{kl} - \alpha\theta\delta_{kl}), \ (\theta = T - T_0) \tag{6}$$

where σ_{ij} is the stress tensor; C_{ijkl} is the elastic constant tensor which depends on the crystal structure; α is the

View Article Online

Published on 23 May 2023. Downloaded by Xiamen University on 4/11/2024 1:34:50 PM.

Table 1 Major physical properties for the temperature calculations

Properties	Value and unit
Density of the graphite crucible	1730 kg m^{-3}
Density of the insulation layer	200 kg m^{-3}
Density of the 4H-SiC crystal	3220 kg m^{-3}
Heat capacity of the graphite crucible	2250 J kg^{-1} K^{-1}
Heat capacity of the insulation layer	1000 J kg^{-1} K^{-1}
Heat capacity of the 4H-SiC crystal	1281 J kg^{-1} K^{-1}
Thermal conductivity of the graphite crucible	22.3 + (2.3 × 10^7)/(1 + (T/0.00056)) W m^{-1} K^{-1}
Thermal conductivity of the insulation layer	0.193 × exp(0.00079 × (T − 273)) W m^{-1} K^{-1}
Thermal conductivity of the 4H-SiC crystal	4.517 × 10^5/($T^{1.29}$) W m^{-1} K^{-1}
Emissivity of the wall	0.8
Emissivity of the graphite crucible	0.8
Emissivity of the insulation layer	0.8
Emissivity of the 4H-SiC crystal	0.8

thermal expansion coefficient; ε_{kl} and δ_{kl} are the strain tensor and Kronecker delta tensor, respectively.

SiC crystals grown by sublimation have a cylindrical shape and can be approximately identified as axisymmetric. Thus, the relation between strain and displacement can be expressed as:

$$\varepsilon_{rr}=\frac{\partial u_r}{\partial r},\varepsilon_{\theta\theta}=\frac{u_r}{r},\varepsilon_{zz}=\frac{\partial u_z}{\partial z},\quad \varepsilon_{rz}=\frac{\partial u_r}{\partial z}+\frac{\partial u_z}{\partial r},\varepsilon_{r\theta}=\varepsilon_{\theta z}=0 \tag{7}$$

where u_r and u_z are the displacement in the radial direction and the displacement in the axial direction, respectively. Based on the assumption of symmetry, the displacement in the angular direction is zero, therefore $\sigma_{\theta z}$ and $\sigma_{\theta r}$ are not calculated.

The stress balance equation in cylindrical coordinates in the axisymmetric case can be expressed as:

$$\frac{\partial\sigma_{rr}}{\partial r}+\frac{\partial\sigma_{rz}}{\partial z}+\frac{\partial_{rr}-\sigma_{\theta\theta}}{r}=0,\quad \frac{\partial\sigma_{rz}}{\partial r}+\frac{\partial\sigma_{zz}}{\partial z}+\frac{\sigma_{rz}}{r}=0 \tag{8}$$

The 4H-SiC single crystal has a hexagonal structure, so its elastic matrix has only five independent components. Assuming T_0 = 293.15K, the stress–strain relation in cylindrical coordinates can be represented as:

$$\begin{pmatrix}\sigma_{rr}\\ \sigma_{\theta\theta}\\ \sigma_{zz}\\ \sigma_{rz}\end{pmatrix}=\begin{pmatrix}C_{11}&C_{12}&C_{13}&0\\ C_{12}&C_{11}&C_{13}&0\\ C_{13}&C_{13}&C_{33}&0\\ 0&0&0&C_{44}\end{pmatrix}\begin{pmatrix}\varepsilon_{rr}-\alpha(T-T_0)\\ \varepsilon_{\theta\theta}-\alpha(T-T_0)\\ \varepsilon_{zz}-\alpha(T-T_0)\\ \varepsilon_{rz}\end{pmatrix} \tag{9}$$

The von Mises stress is used to show the thermoelastic stress in a crystal. The von Mises stress is calculated by:

$$\sigma_{\mathrm{von}}=\sqrt{\frac{(\sigma_{rr}-\sigma_{zz})^2+(\sigma_{rr}-\sigma_{\theta\theta})^2+(\sigma_{zz}-\sigma_{\theta\theta})^2+6\sigma_{rz}{}^2}{2}} \tag{10}$$

And the equivalent force used to calculate the dislocation density is expressed in terms of the second invariant of the stress bias:

$$\sqrt{J_2}=\frac{\sqrt{3}}{3}\sigma_{\mathrm{von}} \tag{11}$$

For the calculation of the thermal stress field in SiC crystals, the boundary conditions are described as follows:

(a) There is no stress from the seed and seed holder at the top of the crystal; (b) neglecting the interaction of the equidistant rings on the sides of the crystal. Both above boundary conditions can be described as $\vec{\sigma}\cdot\vec{n}=0$.

The thermophysical properties used for simulations are listed in Table 2.[10]

2.4 Dislocation dynamics

The Alexander–Haasen model describes the time evolution of the mobile dislocation density N_m and plastic strain components ε_{ij}^p:

$$\frac{\mathrm{d}N_\mathrm{m}}{\mathrm{d}t}=K\nu N_\mathrm{m}\tau_{\mathrm{eff}}^{\lambda} \tag{12}$$

$$\frac{\mathrm{d}\varepsilon_{ij}^p}{\mathrm{d}t}=\frac{b\nu N_\mathrm{m}}{2\sqrt{J_2}}S_{ij} \tag{13}$$

$$\nu=k_0\tau_{\mathrm{eff}}^m\exp\left(-\frac{Q}{k_\mathrm{b}T}\right) \tag{14}$$

where ν is the slip velocity of dislocation; τ_{eff} is the effective stress representing the contribution of stress from the dislocation; b is the Burgers vector; S_{ij} is the deviatoric stress tensor; J_2 is the second invariant of the deviator stress tensor; Q is the activation enthalpy; k_b is the Boltzmann constant; and K, λ, m, and k_0 are constants related to materials.

The expression for the effective stress can be expressed as a function of the maximum value

$$\tau_{\mathrm{eff}}=\max\left(\sqrt{J_2}-D\sqrt{N_\mathrm{m}}-\tau_{\mathrm{crit}},0\right) \tag{15}$$

where D is the hardening factor which depends on the materials;[18] an additional term τ_{crit} was introduced, which

Table 2 Parameters for the thermal stress calculations

Symbol	Description	Value and unit
T_0	Reference temperature	293.15 K
α	Thermal expansion coefficients	4.5 × 10^{-6} 1/K
C_{11}	Elasticity constants	−0.025 GPa × T + 486.6 GPa
C_{12}	Elasticity constants	−0.011 GPa × T + 101.3 GPa
C_{13}	Elasticity constants	−0.011 GPa × T + 59.02 GPa
C_{33}	Elasticity constants	−0.025 GPa × T + 528.9 GPa
C_{44}	Elasticity constants	−0.007 GPa × T + 150.3 GPa

This journal is © The Royal Society of Chemistry 2023

Published on 23 May 2023. Downloaded by Xiamen University on 4/11/2024 1:34:50 PM.

represents the stapling effect of impurity atoms on dislocations;[16,17] the magnitude of the stress was described in the literature as being influenced by the concentration of impurities. In a sense, if $\sqrt{J_2} - D\sqrt{N_m} - \tau_{crit} \leq 0$ then the dislocation multiplication rate in the A–H model $dN_m/dt = 0$. Reference values for the τ_{crit} magnitudes in the specific cases will be given in the subsequent discussions. The boundary condition of dislocation calculation is set to zero flux, the initial dislocation density N_0 is set to 1 (cm^{-2}) and the initial dislocation multiplication rate $dN_m/dt = 0$. The parameters used for dislocation calculations are listed in Table 3.[9]

2.5 Calculation error

In this paper, the authors separately solve the thermal field, thermal stress field, and dislocation density, and this section will analyse the error of these three parts.

The heat transfer calculation part was mainly verified by grid sensitivity. We used different sizes of grids for the calculation of the thermal field. We found that the difference in the global temperature distribution was tiny or could be considered no different when the grid number is larger than 19 904. By verifying grid sensitivity, we believed that the calculation error of the heat field was within the acceptable range and did not affect the subsequent calculations.

The thermal stress calculation is based on the thermoelastic theory, and we solve the thermal stress field by the magnitude of the temperature gradient. We consider the result as the analytical solution rather than the numerical solution because the stress field is solved by associating the overall stiffness matrix with the load matrix to solve the displacement of each node and then solving the stress by the elastic equation. The mesh size only affects the accuracy of the solution and does not introduce numerical errors.

The magnitude of the dislocation density is directly related to thermal stress. The dislocation density solved in the form defined by the equation is also considered an analytical rather than a numerical solution. However, since the parameters of the Alexander–Haasen model are taken from the literature,[9] researchers fit these parameters through experimental and simulation results, they should deviate from the actual situation, so we consider that the solution results do not have numerical errors but parameter errors.

Table 3 Parameters for the dislocation calculations

Symbol	Description	Value and unit
b	Burgers vector	3.073×10^{-10} m
λ	Stress exponential factor	1.1 at $T > 1000$ °C
		0.6 at $T < 1000$ °C
m	Stress exponential factor	2.8
Q	Activation enthalpy	3.3 eV at $T > 1000$ °C
		2.6 eV at $T < 1000$ °C
ν	Dislocation velocity	m s^{-1}
K	Multiplication constant	7.0×10^5
N_m	Mobile dislocation density	m^{-2}
τ_{eff}	Effective stress	Pa
τ_{crit}	Doping stress	Pa
D	Hardening factor	$\frac{b(C_{11}-C_{13})}{4\pi(1-\nu)}$
T	Temperature	K
k_0	Material constant	8.5×10^{-15}
k_b	Boltzmann constant	8.615×10^{-5} eV K^{-1}

2.6 Experimental

A 4-inch SiC crystal was grown by the PVT method, during which nitrogen was used for n-type doping. The monocrystalline substrate was fabricated from the grown crystal ingot through processing processes such as wire cutting, grinding, and polishing. The wafer resistivity was measured by non-contact measurements using a low resistance tester model LEI-1510EA, which measures the resistivity distribution by fully automatically sampling 49 points on the wafer surface. The substrate was etched with molten KOH at 540 °C for 20 minutes, and the density of the dislocation distribution was scanned and counted using an automatic dislocation scanner (LFM-SiC I).

3. Results and discussion

3.1 Calculated dislocations

The crucible heating system was inductively heated with electromagnetic heat as a heat source for SiC crystal growth, the coil power was set to 10.9 kW, and the thermal field calculations for the global model were performed using COMSOL frequency-domain steady-state studies at 10 kHz. Fig. 3 shows the temperature distribution of the global model of the SiC crystal grown by the PTV method. The highest temperature is 2530 K at the bottom corner of the crucible. The lowest temperature is the temperature of the cooling water in the cooling pipe of the copper coil at 300 K. The heat is transferred from the growth chamber to the exterior by thermal conduction and radiation, and the temperature field stabilizes when the interior and exterior reach thermal equilibrium. The axial temperature gradient in the growth chamber is the primary driving force of the SiC crystal growth. In contrast, the radial temperature gradient on the surface of the seed crystal is the underlying cause of thermal stress.

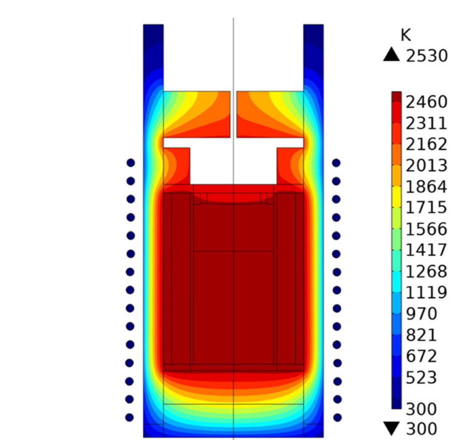

Fig. 3 Temperature distribution in the global model.

View Article Online

Published on 23 May 2023. Downloaded by Xiamen University on 4/11/2024 1:34:50 PM.

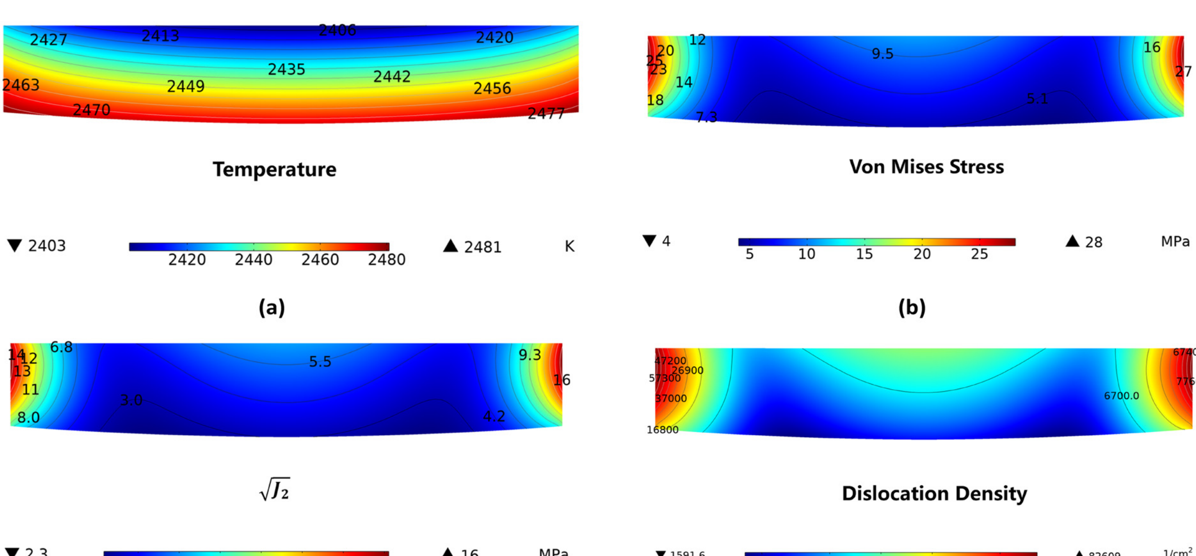

Fig. 4 Temperature, stress and dislocation fields in the SiC ingots: (a) temperature distribution, (b) von Mises stress distribution, (c) 0.5th power of the second invariant of the deviator stress tensor: $\sqrt{J_2}$, (d) dislocation density distribution.

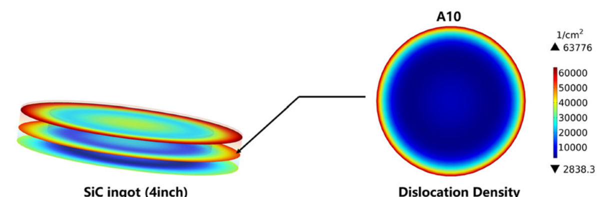

Fig. 5 Computed dislocation density at the locations of the experimental slices.

The generation and proliferation of dislocations during PVT growth are attributed to the nonlinear interaction between thermal stress and dislocations. The temperature, stress, and dislocation density distribution of the ingot during the growth of the SiC crystal were calculated by numerical simulation and shown in Fig. 4(a)–(d). Fig. 4a shows the temperature field in SiC ingots, with the lowest temperature appearing at the center of the bottom of the crystal due to cooling from the pedestal. The highest temperature occurs on the side at the top of the crystal due to the excellent thermal insulation of the side of the crucible. It can be seen that the stress level is relatively steep, as a curved isotherm appears inside the crystal and the maximum temperature difference reaches 78 K.

Fig. 4b and c show the distribution of thermal stresses in the ingot, with the maximum stress occurring at the edge of the crystal due to the most significant radial temperature gradient. The minimum stress occurs near the axisymmetric line at the lower part of the crystal.

Fig. 4d shows the dislocation density distribution in the crystal, and the distribution of dislocations follows the same

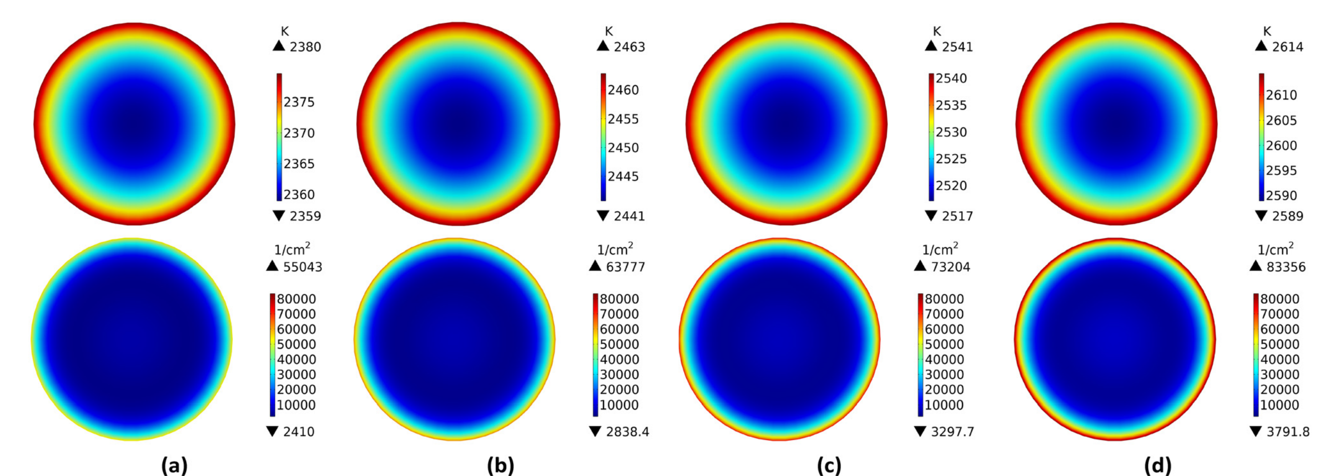

Fig. 6 Dislocation density distribution of SiC wafers at different coil powers: (a) P = 10.0 kW, (b) P = 10.9 kW, (c) P = 11.8 kW, (d) P = 12.7 kW.

 This journal is © The Royal Society of Chemistry 2023

Published on 23 May 2023. Downloaded by Xiamen University on 4/11/2024 1:34:50 PM.

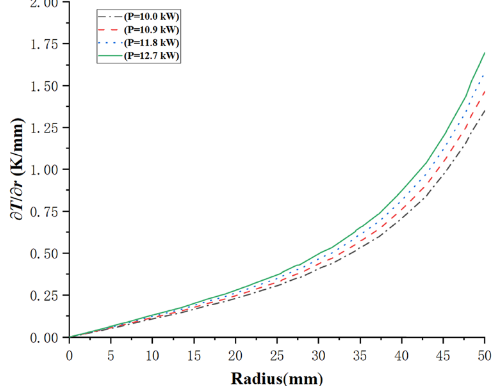

Fig. 7 Radial temperature gradient at different power.

trend as the distribution of thermal stresses. The results imply that the heating flux near the edges of the crystal should be reduced to decrease the dislocation density during the growth process.

3.2 Effect of temperature on dislocation density

Fig. 5 shows the position of the SiC wafer slices during the experiment through a 3D view, with A10 in the figure representing the tenth slice counted from the bottom of the crystal, which shows the dislocation density of the pieces. It should be noted that the dislocation density calculated here does not yet consider the effect of nitrogen impurities on dislocation density. To investigate the effect of temperature on the dislocation density distribution, Fig. 6a–d show the temperature and dislocation density distribution on the surface of the SiC wafer at different coil powers. As the coil power increases, the temperature of the wafer surface increases. The calculated results show that the maximum and minimum values of dislocation density increase with the temperature rise, and the dislocation cloud at the edge of the wafer gradually changes from green to red.

This phenomenon can be explained as follows: an increase in the coil power leads to a rise in the global temperature and the wafer surface temperature. Fig. 7 shows the radial temperature gradient distribution pattern along the radius direction for different coil powers. The coil power is positively correlated with the value of the temperature gradient, which differs less at the center and more at the edges. The minimum value of the dislocation density near the center differs by only about 1000 cm^{-2} for the four heating powers, while the maximum value at the edges differs by nearly 30 000 cm^{-2}. The larger the temperature gradient, the larger the deal of thermal stress, which increases dislocations.

3.3 Effect of nitrogen doping on dislocation density

In the experiment, SiC crystals were grown in an atmosphere of nitrogen, which was adsorbed onto the growing surface to form the n-type SiC. Fig. 10a clearly shows the nitrogen doping during the experiment and can be seen to create a uniquely colored circle at the edge of the wafer. The interface between nitrogen-doped and undoped states is visible.

To consider the effect of nitrogen impurities on dislocation proliferation, we consider the stress term τ_{crit} associated with the impurity atoms in the AH model and consider this term in the region corresponding to the experimental results. The distribution of dislocation density was output by taking different τ_{crit} values employing COMSOL parametric calculations as shown in Fig. 8.

Fig. 8a–f shows that the dislocation density on the surface of the SiC wafer decreases as the value of τ_{crit} increases. The

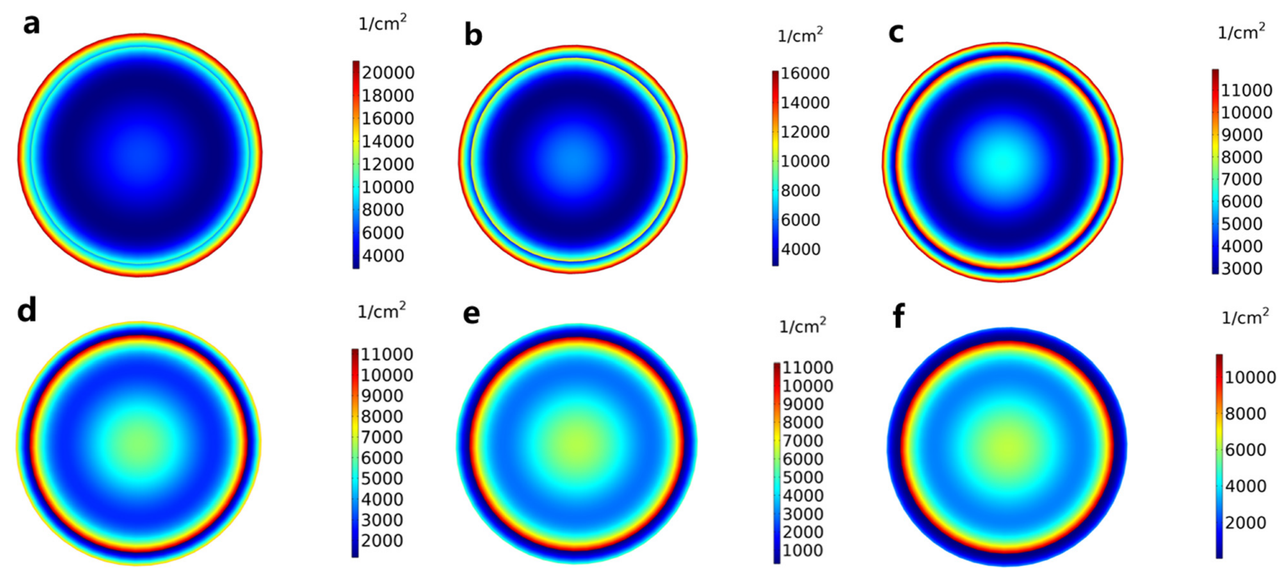

Fig. 8 Dislocation density distribution of SiC wafers at different τ_{crit}: (a) τ_{crit} = 1 MPa, (b) τ_{crit} = 2 MPa, (c) τ_{crit} = 3 MPa, (d) τ_{crit} = 4 MPa, (e) τ_{crit} = 5 MPa and, (f) τ_{crit} = 6 MPa.

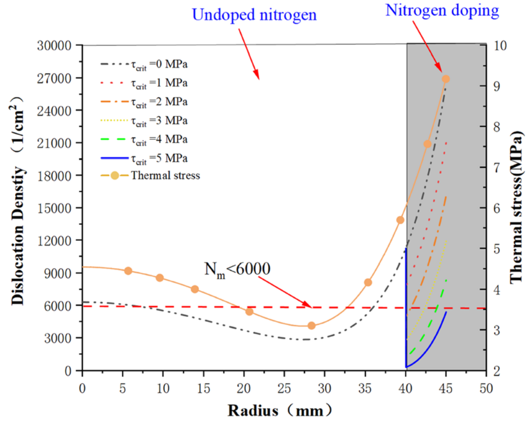

Fig. 9 Variation of the dislocation density in the radius direction for different τ_{crit}.

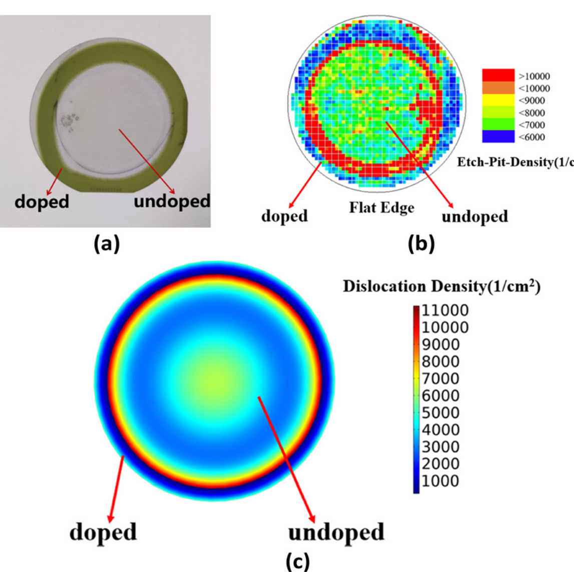

Fig. 10 Experimental and simulation results: (a) nitrogen-doped SiC wafers, (b) etch-pit-density (EPD) distribution measured by the experiment, and (c) dislocation density distribution calculated by the simulation (τ_{crit} = 5 MPa).

AH model can explain: τ_{crit} represents the contribution of the impurity atoms to the effective stress of the dislocation motion, and as τ_{crit} increases, the stress required to generate dislocations increases, and the dislocation density decreases as τ_{crit} increases for the same stress level. It can also be seen from the dislocation cloud diagram that the initial red color at the edge gradually changes to blue color, and when τ_{crit} is taken to more than 5 MPa, the overall dislocation density at the border is less than 6000 cm^{-2}.

Fig. 9 shows more clearly the variation of the dislocation density magnitude along the radius for different values of τ_{crit}. The dislocation density undergoes a sudden shift at the doped and undoped interface, and the impurity atoms play a hindering role in dislocation proliferation.

3.4 Experimental comparison

Fig. 10 shows the experimental and calculation results of the SiC wafer, where all results correspond to the A10 slices in Fig. 5. Fig. 10a shows the interface between the doped and undoped nitrogen atoms, with a clear color difference between the wafer edge and the center. Fig. 10b shows the distribution and magnitude of the EPD density on the SiC wafer. The color legend indicates that the overall EPD density at the doping boundary (undoped nitrogen atoms) is more than 10 000 cm^{-2}. In the doped region, the EPD density is reduced due to the impurity pegging effect on the dislocations and is less than 6000 cm^{-2} overall. The resistivity measurements show that in the nitrogen-doped region (wafer edge region), the resistivity magnitude is below 3 mΩ cm, while in the undoped region, the resistivity magnitude is between 5 mΩ cm and 19 mΩ cm. Fig. 10c shows the dislocation density distribution on the wafer surface obtained from simulations considering impurity doping when τ_{crit} is taken to be 5 MPa. Based on the curve results in Fig. 9 combined with Fig. 10, when τ_{crit} is assumed to be 5 MPa, the simulation results are similar to the experimentally measured data. It is also clear from the simulation results that at the nitrogen-doped interface, the dislocation density undergoes a spatially abrupt decrease from above 10 000 cm^{-2} to below 6000 cm^{-2}.

Conclusions

In this work, the temperature field and stress distribution have been calculated. Based on the thermal stress distribution, the dislocation density distribution has been calculated. To better calculate the dislocations in n-type 4H-SiC, we introduced an effective stress of nitrogen and calculated the stress drop due to the nitrogen doping. Since there is no relevant literature on the effective stress of nitrogen, we performed several calculations of dislocation density with different values of effective stress. Through the experimental comparison, an effective stress of 5 MPa is proposed, which is applicable to the calculation of the dislocation density of 4H-SiC at a certain doping concentration (resistivity less than 3 mΩ cm). This work provides a basis for the calculations and predictions of n-type 4H-SiC crystals in the future.

Conflicts of interest

There are no conflicts to declare.

Acknowledgements

This work is supported by the National Natural Science Foundation of China (Grant No. 52202189, U20A20293, U22A2075, 62274143, 61721005), the "Pioneer" and "Leading Goose" R&D Program of Zhejiang (Grant No. 2022C01021, 2023C01010), the National Key Research and Development Program of China (Grant No. 2018YFB2200101) and the

Published on 23 May 2023. Downloaded by Xiamen University on 4/11/2024 1:34:50 PM.

This journal is © The Royal Society of Chemistry 2023

Published on 23 May 2023. Downloaded by Xiamen University on 4/11/2024 1:34:50 PM.

Zhejiang University Education Foundation Global Partnership Fund.

References

1 X. She, A. Q. Huang, O. Lucia and B. Ozpineci, *IEEE Transactions on Industrial Electronics*, 2017, **64**, 8193–8205.
2 F. Wang and Z. Zhang, *CPSS Trans. Power Electron. Appl.*, 2016, **1**, 13–32.
3 Y. Huang, R. Wang, Y. Qian, Y. Zhang, D. Yang and X. Pi, *Chin. Phys. B*, 2022, **31**, 046104.
4 T. Kimoto and J. A. Cooper, *Fundamentals of silicon carbide technology: growth, characterization, devices and applications*, John Wiley & Sons, 2014, pp. 11–38.
5 P. Haasen, Zur plastischen Verformung von Germanium und InSb, *Z. Phys.*, 1962, **167**, 461–467.
6 I. Yonenaga and K. Sumino, *Phys. Status Solidi A*, 1978, **50**, 685–693.
7 N. Bános, J. Friedrich and G. Müller, *J. Cryst. Growth*, 2008, **310**, 501–507.
8 B. Gao and K. Kakimoto, *J. Cryst. Growth*, 2014, **386**, 215–219.
9 B. Gao and K. Kakimoto, *Cryst. Growth Des.*, 2014, **14**, 1272–1278.
10 B. D. Nguyen, A. M. Rausch, J. Steiner, P. Wellmann and S. Sandfeld, *J. Cryst. Growth*, 2020, **532**, 125414.
11 Q.-S. Chen, P. Zhu and M. He, *J. Cryst. Growth*, 2020, **531**, 125380.
12 P. Zhu, Q.-S. Chen and V. Prasad, *Mater. Today Commun.*, 2021, **27**, 102349.
13 Q. S. Chen, V. Prasad, M. Balkaş and N. Yushin, *J. Heat Transfer*, 2001, **123**, 1098–1109.
14 D. Hofmann, M. Heinze, A. Winnacker, F. Durst, L. Kadinski, P. Kaufmann, Y. Makarov and M. Schäfer, *J. Cryst. Growth*, 1995, **146**, 214–219.
15 H. Luo, X. Han, Y. Huang, D. Yang and X. Pi, *Crystals*, 2021, **11**, 1581.
16 C. T. Tsai, O. W. Dillon, Jr. and R. J. De Angelis, *J. Eng. Mater. Technol.*, 1990, **112**, 183–187.
17 N. Miyazaki and S. Okuyama, *J. Cryst. Growth*, 1998, **183**, 81–88.
18 S. Karpov, A. Kulik, M. Ramm and Y. Makarov, *Mater. Sci. Forum*, 2003, **433–436**, 297–300.